

Quantum chemical roots of machine-learning molecular similarity descriptors

Stefan Gugler and Markus Reiher*

*ETH Zürich, Laboratorium für Physikalische Chemie,
Vladimir-Prelog-Weg 2, 8093 Zürich, Switzerland*

July 7, 2022

Abstract

In this work, we explore the quantum chemical foundations of descriptors for molecular similarity. Such descriptors are key for traversing chemical compound space with machine learning. Our focus is on the Coulomb matrix and on the smooth overlap of atomic positions (SOAP). We adopt a basic framework that allows us to connect both descriptors to electronic structure theory. This framework enables us then to define two new descriptors that are more closely related to electronic structure theory, which we call Coulomb lists and smooth overlap of electron densities (SOED). By investigating their usefulness as molecular similarity descriptors, we gain new insights in how and why Coulomb matrix and SOAP work. Moreover, Coulomb lists avoid the somewhat mysterious diagonalization step of the Coulomb matrix and might provide a direct means to extract subsystem information that can be compared across Born-Oppenheimer surfaces of varying dimension. For the electron density we derive the necessary formalism to create the SOED measure in close analogy to SOAP. Since this formalism is more involved than that of SOAP, we review the essential theory, but also introduce a set of approximations that eventually allow us to work with SOED in terms of the same implementation available for the evaluation of SOAP.

1 Introduction

A molecular descriptor — in the machine-learning literature also known as feature¹ — is a representation of a molecule in terms of a computer readable

*Corresponding author; e-mail: markus.reiher@phys.chem.ethz.ch

vector. Molecular descriptors can be compared in order to assess the similarity of molecules of different composition and configuration. A similarity measure is a mathematical metric, i.e., a function that measures the distance between two points in descriptor space. The closer the two points are, the more similar they are.

A kernel function generalizes this notion.² Examples are Gaussian kernels or linear kernels.^{1,3} They do not bear physical meaning per se, but assess whether two points are close together according to the measure. Often they are chosen for mathematical convenience (such as radial basis functions based on Gaussians⁴), but they can also be loaded with physical interpretation such as the smooth overlap of atomic positions (SOAP).⁵ Even though the notions of features and kernels are distinct, they are sometimes treated as practically the same, since the physical and chemical properties of systems to be represented are encoded in both the kernel and the feature.

There exists a multitude of molecular descriptors, many originating from the field of cheminformatics: One of the most comprehensive overviews was provided by Todeschini and Consonni,⁶ which, however, does not cover post-2012 descriptors, i.e., those that have gained traction within the recent revival of machine learning and artificial intelligence in chemistry. Todeschini and Consonni⁶ classify the descriptors according to the theory from which they are derived: graph theory, discrete mathematics, physical chemistry, information theory, quantum chemistry, organic chemistry, differential topology, algebraic topology. On top of that, they distinguish how they are processed, namely by statistics, chemometrics, or cheminformatics. The bibliography of their review covers the period between 1741 and 2008 with about 6400 references and 3300 descriptors are listed.⁶

With the advent of modern machine learning in chemistry, several groups have developed descriptors and methods that are better tailored to a particular machine-learning method and harness the latest computational developments more efficiently.

The group of von Lilienfeld proposed various descriptors, most of which can be described as many-body expansions; examples are bag of bonds (BoB),⁷ the atom-in-molecule-based descriptor called "amons",⁸ FCHL⁹ (named after the authors), and the development¹⁰ and assessment^{11,12} of Coulomb matrices, their eigenvalues, or multiple Coulomb matrices per molecule. Huang and von Lilienfeld studied the uniqueness of some of their descriptors.¹³

To establish size-intensive descriptors, Collins studied descriptors for machine learning and how to encode bonds.¹⁴ The molecular-structure-based descriptor SOAP by Csanyi and co-workers has experienced continuous development and is among the most successful ones.^{5,15,16} Ceriotti and co-workers have developed and analyzed physics-inspired molecular representations¹⁷⁻¹⁹ and carried out considerable work in unifying the landscape of descriptors.^{17,20-22} Corminboeuf and co-workers have investigated ways to incorporate the electron density into machine learning procedures.^{23,24}

Molecular similarity descriptors such as Coulomb matrix and SOAP have been used in machine-learning applications as 'rulers' to assign a degree of sim-

ilarity to two different structures. Typically, the structures to be compared can differ significantly and may be taken from across chemical space. However, if we consider the opposite case, namely structures that are clearly related through an elementary reaction step, then we arrive at a somewhat paradoxical situation: while reactant and product are obviously rather similar molecules by construction (as they are related by an elementary reaction step), the connecting transition state structure is even more similar to either product or reactant. Yet, it is well known in electronic structure theory that transition state structures (which represent activated molecules that typically exhibit one or two stretched chemical bonds) present a very different electron correlation problem compared to the stable reactant or product structures. Hence, this example presents a well-defined situation, in which molecular structure similarity seems to be insufficient to also judge on electronic similarity, which governs the molecular properties. As a result, a molecular similarity measure might rightfully determine a transition state structure to be more similar to either side of the reaction arrow, but at the same time miss the fact that its electronic structure will be rather different (as measured, for instance, in terms of electron correlation diagnostics). Another measure might even determine all three structure to be basically identical, which will then ignore all fine-grained differentiation that quantum chemical methods attributes to them.

We note that machine learning has hardly been applied to transition states,^{25–28} but more can be expected in the future in view of the key role transition states play in chemistry. It is therefore important to better understand to what degree descriptors of molecular similarity can differentiate between stable intermediates (i.e., local minima on the Born-Oppenheimer potential energy surface) and transition states (i.e., first-order saddle points on that surface).

In this work, we therefore consider the physical foundations of the Coulomb matrix and SOAP from the point of view of electronic structure theory in order to shed light on this paradox. We will first introduce example reactions for which we will compare the different descriptors. Then, we study a general expression for the electronic energy to which we want to relate the measures in order to establish a relation between a similarity measure and this key quantity of electronic structure theory. Afterwards, we first consider the relation of the electronic energy and the Coulomb matrix, which will also lead us to introduce Coulomb lists as a descriptor. Then, we turn to such a relation for SOAP, which will also lead us to the introduction of a new descriptor, namely the smooth overlap of electron densities.

2 An Elementary Reaction Step Example

By contrast to a typical machine learning study, we will, in this first step, not consider vast amounts of data, but instead make an attempt to understand how Coulomb matrix and SOAP operate at the level of a single elementary reaction step. In order to be able to later extend this work to a large data set, we chose our (generic) example (reaction 1) in such a way that it is on the same

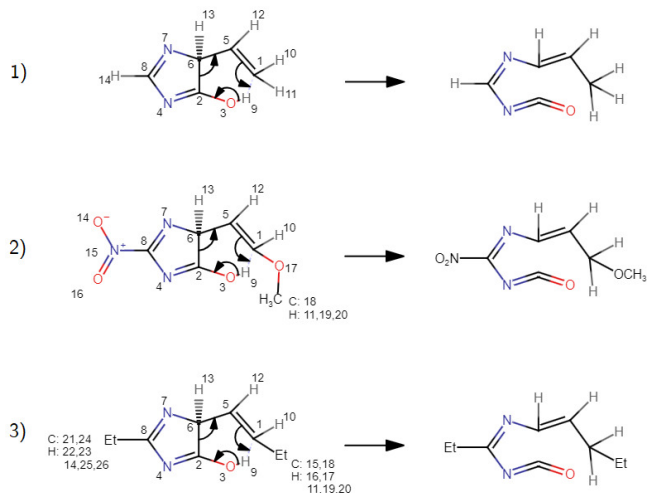


Figure 1: Reactions for which an elementary step relates reactant and product through a transition state structure. In (the generic) reaction 1, the nucleophilic double bond between C₁ and C₅ abstracts the proton of the hydroxyl group, H₉. The C₂-C₆ bond breaks and, hence, opens up the imidazole ring, yielding an isocyanate. Reaction 2 and 3 show analogous reactions with a push-pull system (in 2) and two ethyl substituents (in 3), respectively.

Born-Oppenheimer surface as the QM9 reference data set of von Lilienfeld and co-workers.²⁹

We will base the numerical part of this work on the reactions shown in Figure 1: The nucleophilic double bond between C₁ and C₅ abstracts the proton of the hydroxyl group, H₉, which results in a change of the aromatic system as the imidazole ring opens up. An isocyanate group is created. In this generic reaction 1, electronic and structural changes are both present. This allows us to probe to what extent a descriptor can account for electronic changes in terms of its numerical values.

Analogously to reaction 1, reactions 2 and 3 are chosen as proton abstraction reactions of the same type, but with modulating substituents. In the case of reaction 2, we introduced a push-pull-type π -system structure to replace two hydrogen atoms of the original reaction. The nitro group functions as an electron acceptor and the methoxy group may be considered as the electron donor. Accordingly, this system poses a challenge for a descriptor. In the case of reaction 3, two ethyl groups replace the same two hydrogen atoms to probe the effect of atoms that are farther away from the reactive site. Hence, the three reactions serve the purpose of studying descriptor transferability because the locality of the descriptor should highlight whether the generic reaction 1 can be recovered in reactions 2 and 3.

3 Electronic Energy in Terms of Nuclear Contributions

To connect a descriptor of molecular similarity, which refers to an atom-resolved molecular structure (usually in terms of its nuclear coordinates), with the expression for the electronic energy, we first need to rewrite this energy in terms of nuclear contributions. Although every electronic structure model affords a different expression for the electronic energy, a common expression can be formulated in terms of one- and two-body reduced density matrices. If we focus on the nuclear contributions in such an expression, we may write the electronic energy in Hartree atomic units as:

$$E_{\text{el}} = \sum_{I>J}^M \frac{Z_I Z_J}{|\mathbf{R}_I - \mathbf{R}_J|} - \sum_{i,J}^{N,M} n_i \left\langle \phi_i \left| \frac{Z_J}{|\mathbf{R}_J - \mathbf{r}|} \right| \phi_i \right\rangle + E_{\text{rest}}[\{\phi_i\}], \quad (1)$$

where I and J are the indices running over the M nuclei with their respective nuclear charges, Z_I and Z_J , and coordinates, \mathbf{R}_I and \mathbf{R}_J . The first sum refers to the Coulomb repulsion of all nuclei, which is independent of the electronic structure model.

The second term delivers the potential energy for the interaction with the external potential and all other contributions are kept hidden in the third one. For the sake of simplicity, we have introduced a general occupation number n_i , which can be easily generalized to the doubly-indexed one-body reduced density matrix. One may simply choose the n_i to be all equal to one as in unrestricted Hartree-Fock or Kohn-Sham theory. The index i then runs over N spin orbitals ϕ_i from which the electronic wave function is constructed. Finally, \mathbf{r} is the coordinate of an electron.

$E_{\text{rest}}[\{\phi_i\}]$ denotes the remaining contributions to the electronic energy, namely the expectation values for total kinetic energy, $\langle T \rangle$, and the electron-electron interaction, $\langle V_{\text{ee}} \rangle$,

$$E_{\text{rest}} = \langle T \rangle + \langle V_{\text{ee}} \rangle, \quad (2)$$

which all depend on the wave function and, hence, on all orbitals $\{\phi_i\}$. If molecular orbitals (MOs) are expanded into a set of m basis functions χ_μ ,

$$\phi_i = \sum_{\mu=1}^m c_\mu^{(i)} \chi_\mu, \quad (3)$$

their corresponding MO coefficients $c_\mu^{(i)}$ will enter the energy expression

$$E_{\text{el}} = \sum_{I>J}^M \frac{Z_I Z_J}{|\mathbf{R}_I - \mathbf{R}_J|} - \sum_{i,J}^{N,M} n_i \sum_{\mu\nu}^m c_\mu^{(i)} c_\nu^{(i)} \left\langle \chi_\mu \left| \frac{Z_J}{|\mathbf{R}_J - \mathbf{r}|} \right| \chi_\nu \right\rangle + E_{\text{rest}}[\{c_\mu^{(i)}\}]. \quad (4)$$

Note that we assume the basis functions to be real and therefore avoided a denotation for complex conjugation; however, this restriction can be easily lifted.

We re-write the electron-nucleus attraction potential-energy integrals over basis functions χ_μ into a matrix, $\mathbf{V}^{(J)}$, with elements

$$V_{\mu\nu}^{(J)} = \left\langle \chi_\mu \left| \frac{Z_J}{|\mathbf{R}_J - \mathbf{r}|} \right| \chi_\nu \right\rangle \quad (5)$$

and the MO coefficients into vectors, $\mathbf{c}^{(i)}$ and $\mathbf{c}^{(i)}$, obtaining

$$E_{\text{el}} = \sum_{I>J}^M \frac{Z_I Z_J}{|\mathbf{R}_I - \mathbf{R}_J|} - \sum_{i,J}^{N,M} n_i \mathbf{c}^{(i)} \mathbf{V}^{(J)} \mathbf{c}^{(i)} + E_{\text{rest}}[\{c_\mu^{(i)}\}]. \quad (6)$$

Obviously, for a close connection of the quantum chemical foundations to a molecular similarity descriptor of a machine learning model, we may require that a descriptor should be based on Cartesian coordinates of all atomic nuclei, $\{\mathbf{R}_I\}$, of a molecule because these define a molecular structure to which the Born-Oppenheimer approximation assigns an electronic energy. Coulomb matrix and SOAP fulfill this requirement (see below). Moreover, according to the electronic energy expression we require that the descriptor depends on the nuclear charge numbers, which, together with the nuclear coordinates, defines the external potential. The external potential and the number of electrons in the system contain all information to formulate the electronic Hamiltonian and, hence, all information to solve for the electronic energy (E. Bright Wilson argument³⁰). The Coulomb matrix fulfills this requirement by construction, but it should be noted that it involves a diagonalization step that changes the information encoded in a rather intransparent way. However, the standard formulation of SOAP considers molecular structure through fuzzy atoms, where all atoms are considered equal (see below). As such, nuclear coordinates enter the procedure, but their type (in terms of the nuclear charge number) is usually not resolved. According to the first Hohenberg-Kohn theorem,³¹ which is also taken as the basis of density functional theory, there exists a one-to-one correspondence between the external potential and the electron density. Since SOAP constructs a density distribution of molecular structure, one may wonder whether a relation to the electron density (and hence to the electronic energy) can be established. We will consider these matters later on in this work and now first turn to the Coulomb matrix due to its obvious link to the external potential.

4 Coulomb Matrix and Coulomb List

The elements of the Coulomb matrix¹⁰ are defined as

$$C_{IJ} = \begin{cases} \frac{Z_I^{2.4}}{|\mathbf{R}_I - \mathbf{R}_J|} & I = J \\ \frac{2 Z_I Z_J}{|\mathbf{R}_I - \mathbf{R}_J|} & I \neq J. \end{cases} \quad (7)$$

The diagonal in the Coulomb matrix is sometimes referred to as the ‘self-interaction term’,¹¹ even though there is no basis in classical electrodynamics for a self-interaction of a point charge. A pragmatic justification is that the diagonal term conveys information about the identity of the elements. The original publication¹⁰ states that the “diagonal elements encode a polynomial fit of atomic energies to nuclear charge”. Since the authors wanted to predict atomization energies, this diagonal brings relevant information into the problem from a priori knowledge, but makes the descriptor less general and less interpretable. Yet another interpretation³² is linking the diagonal terms to the total potential energy of a neutral atom in the Thomas–Fermi model, which is $E_{\text{TF}} = -0.7687Z^{7/3}$.³³

Molecules of different size, M , will be padded with rows and columns of zeros in their Coulomb matrix representation to match the size of the largest molecule to be compared. The Coulomb matrix itself cannot be used as a descriptor for molecules of different sizes, because it is not permutationally invariant (exchange of rows and columns change the descriptor but physically, the order of the atoms in the molecule does not matter) and different information would be stored in different dimensions of the matrix.

Three remedies have been proposed¹¹ to transform the Coulomb matrix into a permutationally invariant descriptor. The simplest one, which we are going to analyze here, is the eigenspectrum: Calculating the eigenvalues, λ_i and sorting them such that $|\lambda_i| \geq |\lambda_{i+1}|$. This is the original recipe proposed by Rupp *et al.* in 2012.¹⁰ For M atoms, this method reduces the dimensionality from M^2 degrees of freedom to only M . The second option to make the Coulomb matrix permutationally invariant is the sorted Coulomb matrix: The rows (or equivalently, the columns) are sorted by their Euclidean norm, such that $\|C_i\|_2 \geq \|C_{i+1}\|_2$. This leads to an overdetermined system, as the dimensionality is M^2 now and may produce to non-smooth changes in the sorting even for small changes in the coordinates. And the third approach is to represent each system by a set of n sorted Coulomb matrices, each injected with Gaussian noise to vastly augment dimensionality.

4.1 Atomic Descriptors $\mathcal{F}_n^{(J)}$ and $\mathcal{F}_e^{(J)}$

We now split Eq. (6) into atomic contributions by moving the sum over the nuclei in front of the expression

$$E_{\text{el}} = \sum_J^M \left[\mathcal{F}_n^{(J)} - \mathcal{F}_e^{(J)} \right] + E_{\text{rest}} \quad (8)$$

with

$$\mathcal{F}_n^{(J)} = \frac{1}{2} \sum_{I \neq J}^M \frac{Z_I Z_J}{|\mathbf{R}_I - \mathbf{R}_J|} \quad (9)$$

and

$$\mathcal{F}_e^{(J)} = \sum_i^N n_i \mathbf{c}^{(i)} \mathbf{V}^{(J)} \mathbf{c}^{(i)} \quad (10)$$

(recall that all n_i are equal to one for unrestricted Hartree-Fock theory and unrestricted Kohn-Sham theory).

Figure 2 depicts the features $\mathcal{F}_e^{(J)}$ and $\mathcal{F}_n^{(J)}$ obtained for reaction 1 of Figure 1. In each subplot of Figure 2, we separated the elements due to the large difference in scale. In (a), the external potential features, $\mathcal{F}_e^{(J)}$, are shown, in (b), the nuclear repulsion features, $\mathcal{F}_n^{(J)}$. The same plot scaled by the respective nuclear charge can be found in the Supporting Information. The scaling only changes the relationship between different elements but not within one group of elements.

We see how the reaction details can be recovered in the plots of Figure 2. For instance, C₆ and C₂ (and similarly H₁₃) show a big drop from the transition state (TS) structure (blue line) to the product (red line) which monitors that the bond between these two atoms is broken. Similarly, H₉ features the biggest relative drop toward the product, which is due to the H shift observed in the reaction. Only for H₁₂ is the product feature higher in energy than those of the TS structure and the reactant. The fact that the reactant and the TS structure features are close together while the product features are separated hints at a possible early TS structure, which resembles the reactant rather than the product according to Hammond’s Postulate.³⁵

To further elucidate the correlation, we plot $\mathcal{F}_n^{(J)}$ and $\mathcal{F}_e^{(J)}$ against each other for each element in Figure 3. Apart from the scaling, the trends are very similar: Not only are all elements of the same type almost linearly correlated but the trend also holds over the course of the reaction (connected points). So apart from small deviations, the nuclear features encode very similar information to the external potential. Since the latter is much more expensive to calculate, it is a good trade-off to use the nuclear features, which are much more cost effective. This is evidence that at least approximatively, only one of the two features can be used without great loss of accuracy. Since the nuclear features are far more efficient to calculate, since they do not depend on a converged SCF calculation, we will solely consider $\mathcal{F}_n^{(J)}$ in what follows.

To compare the effects of different substituents, we plotted the same representations as in Figure 2 in Figure 4. In reaction 2 with the ethyl substituents, we can see that both proximal carbon atoms, C₁₅ and C₂₁, are of similar magnitude, as are the distal carbon atoms, C₁₈ and C₂₁. The patterns of C₆ and C₂ toward the product remain the same. Note that the relative pattern, e.g., the increase from C₈ to C₆ in reaction 1 but the decrease in the same two carbon atoms in reactions 2 and 3, should not be overinterpreted as this pattern is only dependent on the sorting and does not carry physical meaning. Even for reaction 3 with the electron donating and withdrawing groups, a similar pattern is observed.

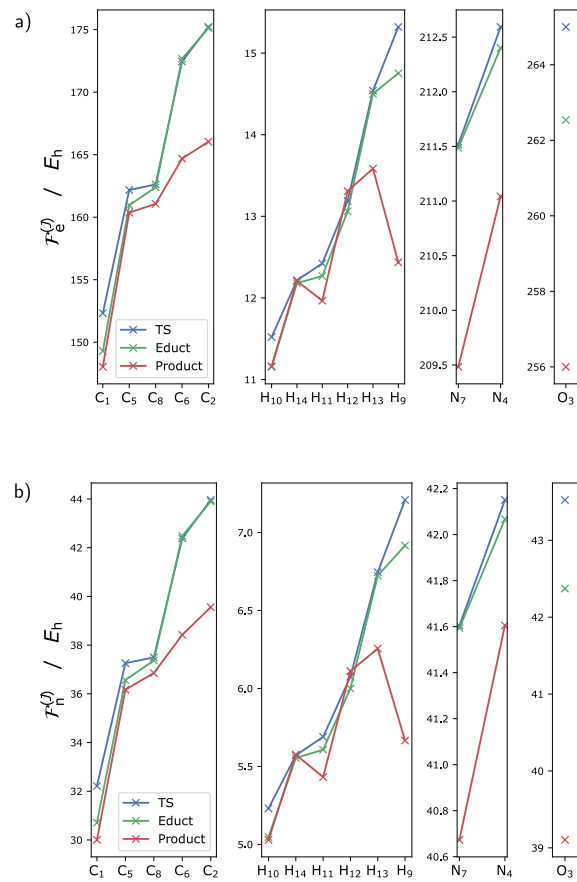


Figure 2: For reaction 1 of Figure 1: (a) external potential features, $\mathcal{F}_e^{(J)}$, and (b) nuclear repulsion features, $\mathcal{F}_n^{(J)}$, in hartree (E_h) (TS denoted in blue, reactant and product in green and red, respectively) The four subplots are sorted by element and the ordering in each subplot according to increasing value of the TS structure feature.

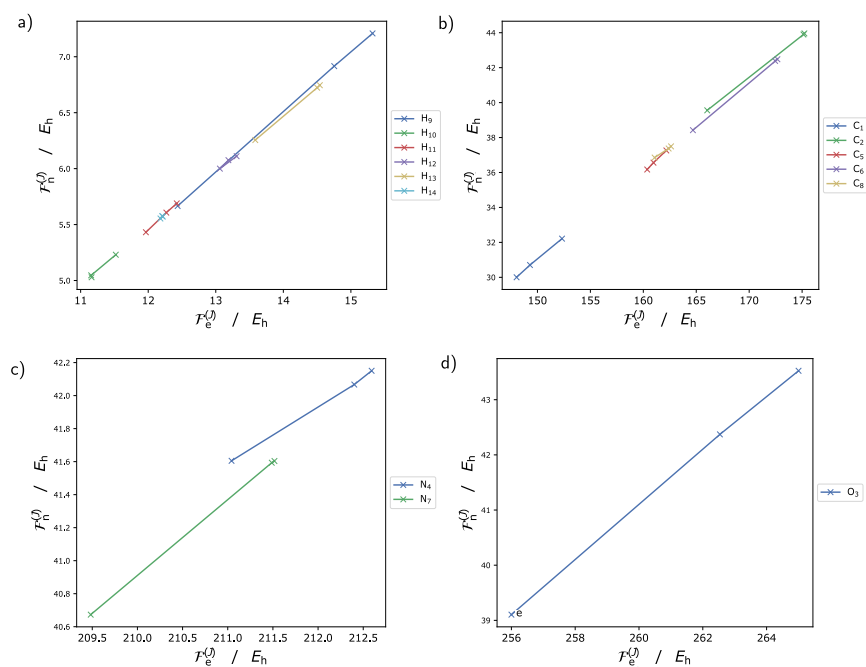


Figure 3: For each element in the reaction 1 from Figure 1, hydrogen, carbon, nitrogen, and oxygen in (a)-(d) we show the correlation between the external potential features, $\mathcal{F}_e^{(J)}$, and the nuclear repulsion features, $\mathcal{F}_n^{(J)}$. The connection between three points is over the course of the reaction from reactant to TS structure, to product.

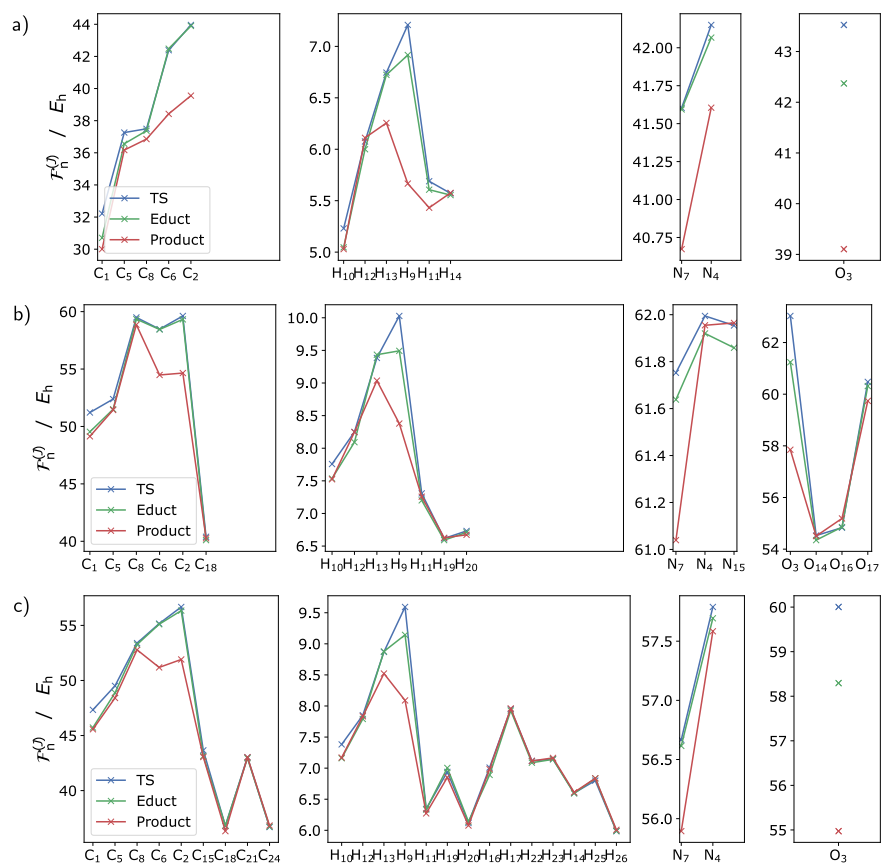


Figure 4: For the reactions of Figure 1, the nuclear repulsion features $\mathcal{F}_n^{(J)}$ are shown (a) for reaction 1 with 'generic' H substituents, (b) for reaction 2 with electron donating and withdrawing groups NO_2 and OCH_3 , and (c) for reaction 3 two ethyl substituents (TS denoted blue, reactant and product as green and red, respectively). The plots are each split into four subplots according to the elemental composition of the reacting molecule.

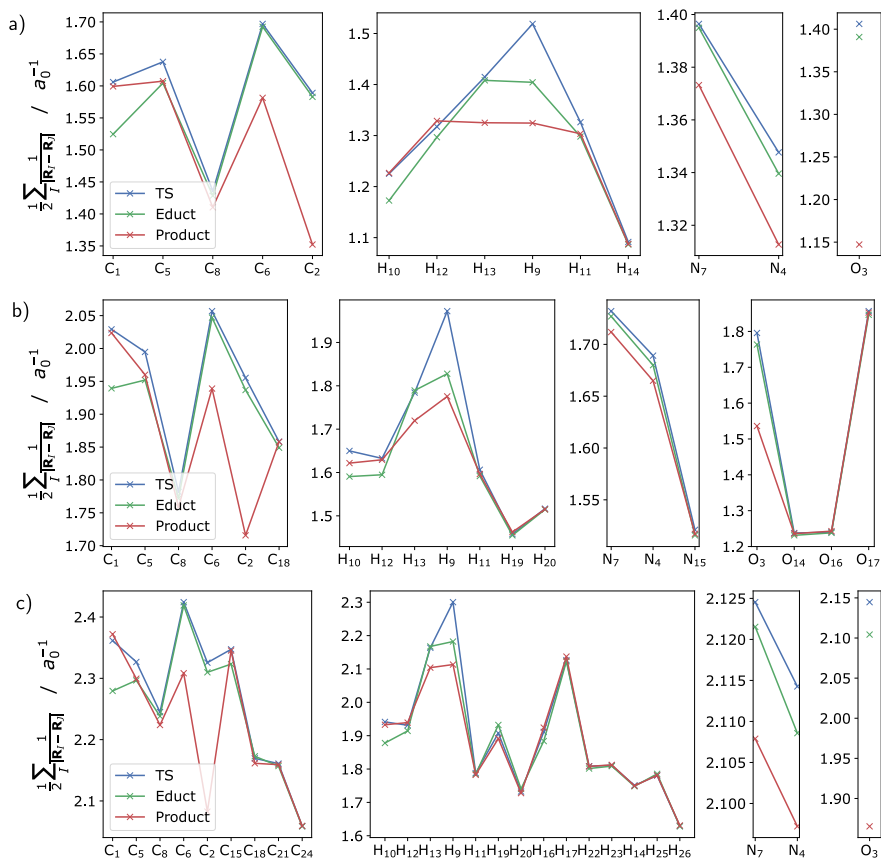


Figure 5: For the reactions of Figure 1, the inverse distance features, $\tilde{\mathcal{F}}_n^{(J)}$ are shown (a) for reaction 1 with H substituents, (b) for reaction 2 with electron donating and withdrawing groups NO₂ and OCH₃, and (c) for reaction 3 with two ethyl substituents (TS denoted blue, reactant and product as green and red, respectively). The plots are each split into four subplots according to the elemental composition of the reacting molecule.

4.2 Relation of $\mathcal{F}_n^{(J)}$ to the Coulomb Matrix

Consider the modified Coulomb matrix, $\tilde{\mathbf{C}}$, with diagonal elements set to 0 and the interaction terms divided by two to resemble avoidance double counting:

$$\tilde{C}_{IJ} = \begin{cases} 0 & I = J \\ \frac{1}{2} \frac{Z_I Z_J}{|\mathbf{R}_I - \mathbf{R}_J|} & I \neq J \end{cases}. \quad (11)$$

All elements $\mathcal{F}_n^{(J)}$ can be obtained by multiplying the J -th row of this Coulomb matrix with 0-diagonal with a vector of one entries, $\mathbf{1}$:

$$\tilde{\mathbf{C}}^{(J)} \cdot \begin{bmatrix} 1 \\ 1 \\ \vdots \\ 1 \end{bmatrix} = \mathcal{F}_n^{(J)}. \quad (12)$$

We have $\mathcal{F}_n^{(J)} = \sum_{I, I \neq J} C_{IJ} = \sum_I \tilde{C}_{IJ}$, establishing a relationship to the (modified) Coulomb matrix \mathbf{C} ($\tilde{\mathbf{C}}$).

To isolate the steric effects from the electronic effects, we consider, similarly to Figure 4 but without the nuclear charges Z_I and Z_J in the numerator, a sum of inverse distances at nucleus J , namely $\tilde{\mathcal{F}}_n^{(J)} \equiv \frac{1}{2} \sum_I \frac{1}{|\mathbf{R}_I - \mathbf{R}_J|}$, in Figure 5. This function has a larger magnitude in areas of the molecule with a higher scaffold density that exhibit more steric effects. For instance, as before, the function shows higher values for C_6 and C_2 and a drastic change toward the product. But by contrast to Figure 4, the function is characterized by a larger value at C_6 than at C_2 because it strictly measures the neighbor density, of which C_6 has more (N_7 , H_{13} , C_5 are nearby) than C_2 (only N_4 and O_3 are nearby). In Figure 4, the larger nuclear charges of nitrogen atoms and oxygen atoms weighted the overall sum higher. More of such effects can be observed: another one is in reaction 2, where the sum of inverse distances at N_{15} is much smaller than in Figure 4 compared to the other nitrogen atoms, since the neighboring oxygen atoms are not weighted according to their nuclear charges.

4.3 Comparison of $\mathcal{F}_n^{(J)}$ and Coulomb Matrix Eigenvalues

In Figure 6, the nuclear repulsion features, $\mathcal{F}_n^{(J)}$, are shown in the left panel and the eigenvalues of the Coulomb matrix, λ_i , in the right panel, all for the intrinsic reaction coordinate (IRC) of reaction 1 in Figure 1. In both feature spaces, it is clearly visible what the TS structure is (step 187) and that it is most likely an early one. The eigenvalues of the Coulomb matrix are hard to interpret, however, since the values are not tied to a particular atom. By contrast, from our $\mathcal{F}_n^{(J)}$ descriptor it is evident which atoms undergo large changes over the course of the reaction: The hydrogen atom that is shifted in the reaction, H_9 , features the largest change in the trace relative to the atoms of the same element. This is in line with Figures 2 and 3, where this hydrogen atom produces the

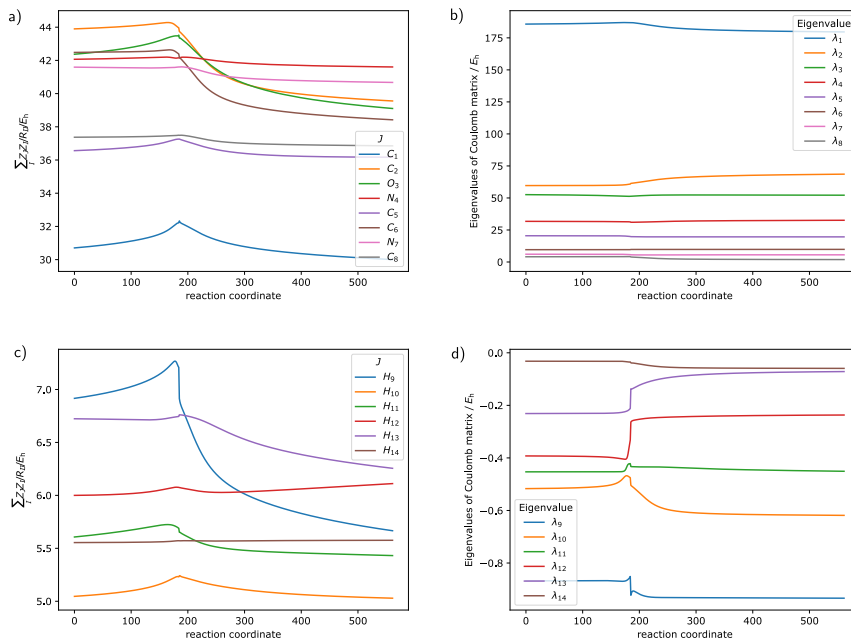


Figure 6: The traces of reaction 1 in Figure 1 over the IRC as represented by $\mathcal{F}_n^{(J)}$ and by the eigenvalues of the Coulomb matrix.

largest spread. As before when discussing Figure 2, we see that C_2 and C_6 behave similarly, as they are the bonding partners of the bond that is broken. The nitrogen atoms, N_4 and N_7 appear relatively stable in terms of the $\mathcal{F}_n^{(J)}$ descriptor apart from a slight relaxation observed in all heavy atoms, due to the molecule opening up and becoming less compact. The carbon atom C_8 with its hydrogen atom H_{14} also show a rather flat trace as they hardly participate in the reaction.

Since $\mathcal{F}_n^{(J)}$ yields interpretable traces and, at the same time, encodes very similar information to that encoded in the eigenvalues of the Coulomb matrix, it represents an excellent alternative, if not a superior type of feature, for many applications. This will be especially interesting if for a given model one wants to backtrack and re-inspect a feature that a machine learning model paid particular attention to. For instance, with such information it is possible to set a threshold of change over the course of the reaction and filter the rest of the data set according to reactions that behave in a similar way. In each case, it is possible to go back to the descriptor and evaluate where a particular contribution came from.

A drawback, however, is that $\mathcal{F}_n^{(J)}$ is not permutationally invariant and suf-

fers from the same issues that plague the plain Coulomb matrix. Due to this very reason, the diagonalization was introduced for the Coulomb matrix (see above), to achieve permutational invariance at the price of interpretability. The reasons given for diagonalizing the Coulomb matrix are:¹⁰ i) the unique encoding, ii) "symmetrically equivalent atoms" are treated the same, iii) invariance with respect to permutation, translation, and rotation and iv) continuous distance. Property i) has been discussed^{34,36} and holds even for homometric molecules, ii) is fulfilled, iii) is a consequence of the ordering, not the diagonalization (there is no intrinsic ordering of eigenvalues as they are complex numbers and the ordering is dependent on the diagonalization algorithm), and iv) is fulfilled. The sorting ensures that the structural properties of each molecule that are compared are of similar size. The caveat is, though, that these structural properties may appear for different chemical reasons.

Since, in the general case, there is no way to track atoms and since this may not even be desirable (as in symmetric molecules certain atoms are symmetry redundant), we have to sort the list (or use any other way to introduce permutational invariance). Therefore, we simply sort the vector $\mathcal{F}_n^{(J)}$ in descending order and ignore tracking of atoms. This is in analogy to the eigenvalues of the Coulomb matrix that are sorted the same way, but the key difference remains: the entries are still atom specific and do not mix information from all atoms (as the diagonalization of the Coulomb matrix does).

Similar to our Coulomb list, in the sorted Coulomb matrix⁷ each element of the matrix is part of the feature, whereas the rows (or columns of this symmetric matrix) are ordered according to their norm. This is equivalent to our approach apart from the fact that there is no summation over the rows (or columns, respectively), leading to a high dimensional feature, which is quadratic in the number of atoms. Moreover, it has been noted that slight variations in atomic coordinates may cause abrupt changes in the Coulomb matrix ordering, thereby impeding the learning of structural similarities.¹¹

Schrier found that the eigenvalues of the Coulomb matrix will not be able to distinguish larger molecules.¹² We do not expect that this is different for the sorted $\mathcal{F}_n^{(J)}$. Furthermore, for macromolecules of more than 10,000 atoms, the global description is not only granular enough but the diagonalization needed for the eigenvalues becomes a true computational bottleneck, as it scales with $\mathcal{O}(M^3)$, while subsequent sorting of is affected by a negligible cost of order $\mathcal{O}(M \log M)$, where M is the number of nuclei.

4.4 Descriptor Extensivity

One long-standing issue in descriptor research is the desired transferability between molecules of different size. Hence, an intensive descriptor is sought for, i.e., one that is independent of molecular size. However, this desire contrasts the inherent extensivity of structures. One approach is to find sub-information that is intensive.

The size (number of elements) of the nuclear repulsion features, $\mathcal{F}_n^{(J)}$, grows

with system size, M . For the specific case of an elementary reaction step, only a very localized part of the system will react while most of the system remains largely unchanged (i.e., internal coordinates of observer atoms change only little), as illustrated by the observer hydrogen atom H_{14} in Figure 6. A simple solution to this problem is to truncate the feature and to consider only to a subset of atoms that vary more than a given threshold and can be considered a relevant subsystem for the process under consideration. More elaborate measures may consider features evaluated in an embedding framework.

However, the issue remains that even if two feature vectors are truncated to the same size to only contain the physically relevant part, they cannot be compared in a direct manner. Only if the set of atoms to which the vector has been truncated to is the same for every system, a direct comparison is possible. The dilemma is that, as soon as convolutions are introduced to achieve permutational invariance, the comparability fades away.

5 Smooth Overlap of Atomic Positions and of Electron Densities

We are advised to compare the results obtained so far to one of the most successful representations for molecular similarity: the SOAP kernel.⁵ In this section, we review the key derivation steps of the SOAP kernel as we need them later to formulate and evaluate our electron-density-based descriptor. In our derivation, we follow Ref. 5, but extend it at key places to highlight important steps of the derivation that are not explicit in the original paper and that become important for our electron-density-based descriptor, for which the derivation must be made more transparent. For this electron-density-based descriptor, we will reinterpret the fuzzy atomic positions of SOAP and generalize them to the actual electron density. Accordingly, we call the resulting descriptor smooth overlap of electron densities (SOED). We emphasize again that the derivation reviewed for SOAP in the next section is necessary as it will turn out to be the key evaluation strategy within our setting to evaluate SOED.

5.1 The SOAP Kernel

SOAP represents a measure for molecular similarity without making any direct connection to the associated electronic energies (by contrast to the Coulomb matrix). A molecule is put with its center of mass at the origin of the coordinate system. We place on each of its atoms I at position \mathbf{R}_I , an unnormalized Gaussian function, g_{α_I} , with parameter $\alpha = 1/(2\sigma_I^2)$, where σ_I is the variance of the Gaussian function at atom I , to obtain a superposition of fuzzy atomic positions,

$$\rho_{\text{mol}}(\mathbf{r}; \{\mathbf{R}_I\}, \{\alpha_I\}) = N_{\text{mol}} \sum_{I=1}^M g_{\alpha_I}(|\mathbf{r} - \mathbf{R}_I|) \quad (13)$$

with the unnormalized Gaussian

$$g_{\alpha_I}(|\mathbf{r} - \mathbf{R}_I|) = \exp\left(-\alpha_I |\mathbf{r} - \mathbf{R}_I|^2\right) \quad (14)$$

and normalization constant N_{mol} to ensure that $\langle \rho_{\text{mol}} | \rho_{\text{mol}} \rangle = 1$. The variable \mathbf{r} is the variable of the field. Note that, in the original publication,⁵ the normalization constant N_{mol} is omitted because later (see below), the kernel will be normalized.

In the original paper,⁵ this superposition has been called 'atomic neighbor density' that represents the 'atomic environment', which we do not adopt here as the superposition in Eq. (13), primarily, does not put an emphasis on some local atomic structure so that other atoms become neighbors or an environment. Instead, it refers to the molecular structure as a whole. Hence, we may refer to it as a 'molecular-scaffold density'. This is also advantageous to conceptually emphasize its relation to our SOED descriptor to be introduced later. The comparison of two molecular-scaffold densities then requires the definition of an overlap measure (see below), which is the origin of the term 'smooth overlap of atomic positions', which we understand as an overlap of molecular scaffolds represented by fuzzy atomic positions.

Usually, the α_I in Eq. (13) are taken to be the same for all atoms, $\alpha_I \rightarrow \alpha$. In some applications, α was optimized as a hyperparameter^{15,38} or simply fixed to some value.^{39,40} Using a different α as a hyperparameter for each element type⁴¹ resulted in the same for each element type.

Notably, the sum in Eq. (13) is permutationally invariant, a property that is important for machine learning: exchanging the terms in the sum does not change the total density. In order to determine the best match of the scaffold densities of two molecules for their comparison regarding the assessment of molecular similarity, it will be necessary to rotate one scaffold density in three-dimensional space with respect to the other. To be able to rotate the sum of Gaussians in Eq. (13), the equation must be expanded into functions dependent on the global polar angles, θ and ϕ (see Figure 7).⁵ In the definition above, they are dependent on \mathbf{r}_A which refers to the frame of reference that is centered on nucleus A and that is not easily rotatable from a global point of view. The functions sought for straightforward rotation of the whole molecular scaffold field⁵ are all to be located at the same single center, which can be the center of mass coordinates of the molecule.

When we multiply out the exponent in Eq. (13), we obtain $-\alpha(\mathbf{r}^2 - 2\mathbf{r} \cdot \mathbf{R}_I + \mathbf{R}_I^2)$, i.e., two squared terms and a cross term. The cross term is then subjected to a Rayleigh expansion of a plane wave in terms of spherical waves,⁵

$$\exp(\mathbf{r} \cdot \mathbf{R}_I) = \sum_{l=0}^{\infty} (2l+1) i_l(rR_I) P_l(\cos \gamma) \quad (15)$$

where i_l is the modified spherical Bessel function of the first kind of degree l and P_l the l th Legendre polynomial, and $\gamma = \angle(\mathbf{r}, \mathbf{R}_I)$, measured from the origin of the coordinate system (see Figure 7). The modified spherical Bessel function of

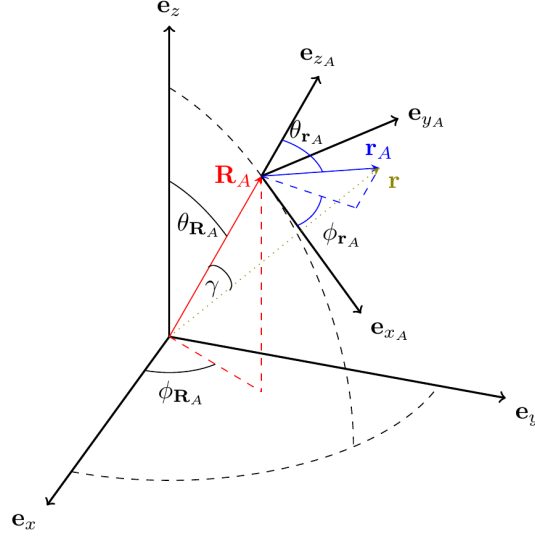


Figure 7: In the global coordinate system, \mathbf{e}_x , \mathbf{e}_y , and \mathbf{e}_z , the angles θ and ϕ denote the polar and azimuthal angles of the field variable $\mathbf{r} \equiv \mathbf{r}(\theta, \phi)$, labeled in green. Nucleus A is at position $\mathbf{R}_A \equiv \mathbf{R}_A(\theta, \phi)$ with polar and azimuthal angles $\theta_{\mathbf{R}_A}$ and $\phi_{\mathbf{R}_A}$. In the coordinate system that is centered on nucleus A , namely \mathbf{e}_{x_A} , \mathbf{e}_{y_A} , and \mathbf{e}_{z_A} , the distance to the field variable is $\mathbf{r}_A = \mathbf{r} - \mathbf{R}_A$ with corresponding polar angles $\theta_{\mathbf{r}_A}$ and $\phi_{\mathbf{r}_A}$. The angle between \mathbf{R}_A and \mathbf{r} is denoted γ .

the first kind, $i_n(x) \equiv \sqrt{\frac{\pi}{2x}} I_{n+1/2}(x)$, is one radial solution to the Helmholtz equation in spherical coordinates and related to the modified Bessel function of the first kind, $I_n(x) \equiv i^{-n} J_n(ix)$, where J_n in turn is the Bessel function of the first kind, which is a solution to Bessel's differential equation, other solutions being the Bessel function of the second kind and Hankel functions. Hence, the molecular scaffold density in Eq. (13) can be expressed as

$$\begin{aligned}
 \rho_{\text{mol}}(\mathbf{r}; \{\mathbf{R}_I\}, \alpha) &= \sum_I^M \exp\left(-\alpha |\mathbf{r} - \mathbf{R}_I|^2\right) \\
 &= \sum_I^M \exp\left(-\alpha (\mathbf{r}^2 - 2\mathbf{r}\mathbf{R}_I + \mathbf{R}_I^2)\right) \\
 &= \sum_I^M \exp\left(-\alpha (r^2 + R_I^2)\right) \sum_{l=0}^{\infty} (2l+1) i_l(2\alpha r R_I) P_l(\cos \gamma),
 \end{aligned} \tag{16}$$

where the normalization constant N_{mol} was omitted as explained above. By

virtue of the spherical harmonics addition theorem,

$$P_l(\cos \gamma) = \frac{4\pi}{2l+1} \sum_{m=-l}^l Y_{lm}^*(\theta_{\mathbf{R}_I}, \phi_{\mathbf{R}_I}) Y_{lm}(\theta, \phi) \quad (17)$$

with angles θ and ϕ as the polar coordinates of the field variable \mathbf{r} measured from the origin and the angles $\theta_{\mathbf{R}_I}$ and $\phi_{\mathbf{R}_I}$ being the polar coordinates of \mathbf{R}_I , notably, also measured from the new common origin. These steps accomplish a single-center expansion necessary for the subsequent rotation in search of best matches of two molecular scaffold densities. We now obtain a compact expression of expansion coefficients and spherical harmonics, where the term $(2l+1)$ cancels out:

$$\begin{aligned} \rho_{\text{mol}}(\mathbf{r}; \{\mathbf{R}_I\}, \alpha) &= 4\pi \sum_I^M \exp(-\alpha(r^2 + R_I^2)) \sum_{l=0}^{\infty} \sum_{m=-l}^{+l} i_l(2\alpha r R_I) Y_{lm}^*(\theta_{\mathbf{R}_I}, \phi_{\mathbf{R}_I}) Y_{lm}(\theta, \phi) \\ &= \sum_I^M \sum_{lm} c_{lm}^I(r; \mathbf{R}_I, \alpha) Y_{lm}(\theta, \phi) \end{aligned} \quad (18)$$

with

$$c_{lm}^I(r; \mathbf{R}_I, \alpha) \equiv 4\pi \exp(-\alpha(r^2 + R_I^2)) i_l(2\alpha r R_I) Y_{lm}^*(\theta_{\mathbf{R}_I}, \phi_{\mathbf{R}_I}) . \quad (19)$$

where \sum_{lm} denotes $\sum_l \sum_{m=-l}^l$. Note that the angular information of the nuclear position is stored in the spherical harmonics $Y_{lm}^*(\theta_{\mathbf{R}_I}, \phi_{\mathbf{R}_I})$. It is exactly these functions that we will need to rotate against each other to generate best overlaps over all possible rotations of the two molecular scaffold densities to be compared. This is due to the fact that the density field is defined in terms of Gaussian functions located at the positions of the nuclei, which therefore need to be rotated. We emphasize this point because it is important for our SOED derivation below and because it appears somewhat obscured in the original paper.⁵ The overlap between these two densities, $\rho_{\text{mol}}(\mathbf{r}; \mathbf{R}_I, \alpha)$ and $\rho'_{\text{mol}}(\mathbf{r}; \mathbf{R}_I, \alpha)$, is defined as the inner product of their densities,

$$S(\rho_{\text{mol}}, \rho'_{\text{mol}}) = \langle \rho_{\text{mol}} | \rho'_{\text{mol}} \rangle = \int_{\mathbb{R}^3} d\mathbf{r} \rho_{\text{mol}} \rho'_{\text{mol}} , \quad (20)$$

where we omitted the parameter dependence for the sake of clarity and $d\mathbf{r} = dx dy dz$. The center of mass of both molecules matches the origin of the coordinate system, leaving rotational freedom around three Euler angles, α, β, γ . Hence, in search for optimal overlaps of the two molecular-scaffold densities we need to integrate over all possible rotations.⁵ This procedure automatically guarantees rotational invariance.

A rotation from the rotation group, $\text{SO}(3)$, can be written as a matrix,

$$\hat{R} \equiv \hat{R}(\alpha, \beta, \gamma) , \quad (21)$$

where α, β, γ are the Euler angles. This rotation operator needs to be integrated over $\text{SO}(3)$ when acting on a density, i.e., all possible rotations of the density must be considered. The volume element on $\text{SO}(3)$ integrating over all possible Euler angles yields the measure

$$d\Omega = \frac{1}{8\pi^2} \sin \beta d\alpha d\beta d\gamma \quad (22)$$

with $\alpha = [0, 2\pi)$, $\beta = [0, \pi)$, and $\gamma = [0, 2\pi)$.

We now need to rotate the spherical harmonic $Y_{lm}(\theta_{\mathbf{R}_I}, \phi_{\mathbf{R}_I})$ in the expansion in Eq. (18). An arbitrary rotation operator, \hat{R} , operating on a spherical harmonic yields a linear combination of new spherical harmonics with a different magnetic quantum number m and the elements of a Wigner D-matrix as expansion coefficients. With this identity, we will rotate the angular information of the nuclear positions (since the radial part is separated) according to

$$\hat{R}Y_{lm}(\theta_{\mathbf{R}_I}, \phi_{\mathbf{R}_I}) = \sum_{m'=-l}^l D_{mm'}^l(\hat{R})Y_{lm'}(\theta_{\mathbf{R}_I}, \phi_{\mathbf{R}_I}) . \quad (23)$$

The elements of the Wigner matrices are given by

$$D_{mm'}^l(\hat{R}) = \left\langle Y_{lm}(\theta_{\mathbf{R}_I}, \phi_{\mathbf{R}_I}) \left| \hat{R} \right| Y_{lm'}(\theta_{\mathbf{R}_I}, \phi_{\mathbf{R}_I}) \right\rangle . \quad (24)$$

This is convenient as the rotation happens in a very compact manner without notational overhead usually involved in rotations. Furthermore, we will see later how multiple Wigner D-matrices will cancel each other out.

When considering the overlap of two molecular-scaffold densities with one of them being rotated,

$$S(\rho_{\text{mol}}, \hat{R}\rho'_{\text{mol}}) = \langle \rho_{\text{mol}} | \hat{R} | \rho'_{\text{mol}} \rangle = \int_{\mathbb{R}^3} d\mathbf{r} \rho_{\text{mol}} \hat{R} \rho'_{\text{mol}} \quad (25)$$

we will have to integrate over all Euler angles α, β, γ , which will yield the rotationally invariant kernel,

$$k(\rho_{\text{mol}}, \rho'_{\text{mol}}; n) = \int_{\alpha, \beta, \gamma} \left| \int_{\mathbb{R}^3} d\mathbf{r} \rho_{\text{mol}} \hat{R} \rho'_{\text{mol}} \right|^n \frac{1}{8\pi^2} \sin \beta d\alpha d\beta d\gamma \quad (26)$$

where we follow the original paper⁵ and artificially introduced the power n as a parameter to be considered later; for now, we set it equal to 1. As we will see in the following, this integral over Euler angles can be evaluated analytically with help of the Wigner D-matrices and will not require us to deal with the explicit rotation algebra as shown in Eq. (23).

We substitute the expanded density of Eq. (18) into the overlap equation, Eq. (25), to obtain the overlap of the two molecular-scaffold densities, where we exploit the rotation identity of Eq. (23),

$$\begin{aligned}
S(\rho_{\text{mol}}, \hat{R}\rho'_{\text{mol}}) &= \int d\mathbf{r} \rho_{\text{mol}} \hat{R}\rho'_{\text{mol}} \\
&= \int d\mathbf{r} \rho_{\text{mol}} \left[\sum_{I'}^{M'} \sum_{l'm'} 4\pi \exp[-\alpha_{I'}(r^2 + R_{I'}^2)] i_{l'}(2\alpha_{I'} r R_{I'}) \hat{R} Y_{l'm'}^*(\Omega_{\mathbf{R}_{I'}}) Y_{l'm'}(\Omega) \right] \\
&= \int d\mathbf{r} \rho_{\text{mol}} \left[\sum_{I'}^{M'} \sum_{l'm'} 4\pi \exp[-\alpha_{I'}(r^2 + R_{I'}^2)] i_{l'}(2\alpha_{I'} r R_{I'}) \right. \\
&\quad \left. \times \sum_{m''=-l'}^{l'} D_{m'm''}^{l'}(\hat{R}) Y_{l'm''}^*(\Omega_{\mathbf{R}_{I'}}) Y_{l'm'}(\Omega) \right] \tag{27}
\end{aligned}$$

where a new coefficient, analogously to Eq. (19) with different indices,

$$c_{l'm''}^{I'} = 4\pi \exp[-\alpha_{I'}(r^2 + R_{I'}^2)] i_{l'}(2\alpha_{I'} r R_{I'}) Y_{l'm''}^*(\Omega_{\mathbf{R}_{I'}}) \tag{28}$$

can be employed to collect many of the terms. Substituting this coefficient and separating the integral into a radial and a spherical part, we obtain

$$\begin{aligned}
S(\rho_{\text{mol}}, \hat{R}\rho'_{\text{mol}}) &= \sum_{I, I'}^{M, M'} \sum_{\substack{l, m \\ l', m'}} \sum_{m''=-l'}^{l'} D_{m'm''}^{l'}(\hat{R}) \underbrace{\int_{r=0}^{\infty} dr r^2 c_{lm}^{I*} c_{l'm''}^{I'}}_{\text{radial}} \\
&\quad \times \underbrace{\int_{\theta=0}^{2\pi} \int_{\phi=0}^{\pi} \sin \phi d\phi d\theta Y_{lm}^*(\Omega) Y_{l'm'}(\Omega)}_{\text{spherical}} \tag{29}
\end{aligned}$$

where we abbreviated the angular information according to $\Omega = (\theta, \phi)$ and $\Omega_{\mathbf{R}_I} = (\theta_{\mathbf{R}_I}, \phi_{\mathbf{R}_I})$. Recall that we also chose to have a general α_I for the unprimed and $\alpha_{I'}$ for the primed molecular scaffolds.

Now, the integral in Eq. (29) must be evaluated. Since the spherical harmonics are orthonormal by definition, the spherical part in Eq. (29) evaluates to

$$\int_{\theta=0}^{2\pi} \int_{\phi=0}^{\pi} \sin \phi d\phi d\theta Y_{lm}^*(\Omega) Y_{l'm'}(\Omega) = \delta_{ll'} \delta_{mm'} . \tag{30}$$

This simplifies the last line in Eq. (29) to the following,

$$S(\rho_{\text{mol}}, \hat{R}\rho'_{\text{mol}}) = \sum_{I, I'} \sum_{l, m} \sum_{m''=-l}^l D_{mm''}^l(\hat{R}) \int_{r=0}^{\infty} dr r^2 c_{lm}^{I*} c_{lm''}^{I'} . \tag{31}$$

setting $m \leftarrow m'$ and $l \leftarrow l'$.

The radial part of the integral in Eq. (29) and Eq. (31) is non-trivial. We first expand it to move the quantities independent of the position before the integral,

$$\int_{r=0}^{\infty} dr r^2 c_{lm}^{I*} c_{lm}^{I'} = (4\pi)^2 \exp(-(\alpha_{I'} R_{I'}^2 + \alpha_I R_I^2)) Y_{lm}(\Omega_{\mathbf{R}_I}) Y_{l'm'}^*(\Omega_{\mathbf{R}_{I'}}) \times \int_{r=0}^{\infty} dr r^2 \exp(-(\alpha_{I'} + \alpha_I) r^2) i_l(2\alpha_I r R_I) i_{l'}(2\alpha_{I'} r R_{I'}) \quad (32)$$

where the integral is solved as

$$\int_{r=0}^{\infty} dr r^2 \exp(-(\alpha_{I'} + \alpha_I) r^2) i_l(2\alpha_I r R_I) i_{l'}(2\alpha_{I'} r R_{I'}) = \frac{1}{4} \left(\frac{\pi}{(\alpha_I + \alpha_{I'})^3} \right)^{1/2} i_l \left(2 \frac{\alpha_I \alpha_{I'}}{\alpha_I + \alpha_{I'}} R_I R_{I'} \right) \exp \left(\frac{\alpha_I^2 R_I^2 + \alpha_{I'}^2 R_{I'}^2}{\alpha_I + \alpha_{I'}} \right) \quad (33)$$

according to Weber.^{42,43}

The prefactor in Eq. (32) can be combined with the result from the integral Eq. (33). If we had considered the two normalization constants $N_{\text{mol}} = (\frac{2\alpha}{\pi})^{3/4}$ that we omitted from Eq. (13), we would have obtained the same overlap as Kaufmann and Baumeister,⁴⁴

$$S(\rho_{\text{mol}}, \hat{R} \rho'_{\text{mol}}) = \sum_{I, I'} \sum_{l, m, m'} D_{mm''}^l(\hat{R}) \tilde{I}_{mm''}^l(\alpha_I, \alpha_{I'}, \mathbf{R}_I, \mathbf{R}_{I'}) \quad (34)$$

with

$$\tilde{I}_{mm''}^l(\alpha_I, \alpha_{I'}, \mathbf{R}_I, \mathbf{R}_{I'}) = 4\pi \left(2 \frac{(\alpha_I \alpha_{I'})^{1/2}}{\alpha_I + \alpha_{I'}} \right)^{3/2} \exp \left(-\frac{\alpha_I \alpha_{I'}}{\alpha_I + \alpha_{I'}} (R_I^2 + R_{I'}^2) \right) \times i_l \left(2 \frac{\alpha_I \alpha_{I'}}{\alpha_I + \alpha_{I'}} R_I R_{I'} \right) Y_{lm}(\Omega_{\mathbf{R}_I}) Y_{l'm''}^*(\Omega_{\mathbf{R}_{I'}}) . \quad (35)$$

For $\alpha \leftarrow \alpha_I$ and $\alpha \leftarrow \alpha_{I'}$, i.e. $\tilde{I}(\alpha, \alpha, \mathbf{R}_I, \mathbf{R}_{I'})$ we recover the result obtained in the original SOAP paper,⁵ which was denoted there $\tilde{I}_{mm''}^l(\alpha, \mathbf{R}_I, \mathbf{R}_{I'})$. The prefactor on the original paper, $\sqrt{\frac{2\pi^5}{\alpha^3}}$, as noted in the erratum,⁴⁵ originates from the missing normalization constants, N_{mol} . If they were included, that new prefactor would not have been necessary, as we can easily verify by $\sqrt{\frac{2\pi^5}{\alpha^3}} N_{\text{mol}}^2 = 4\pi$, and where 4π is their original prefactor. As already noted in the erratum,⁴⁵ this does not produce an error, as it gets cancelled at the normalization step.

In the original paper,⁵ the authors defined a term for the sum over all pairwise interactions of the integral

$$I_{mm''}^l \equiv \sum_{I, I'} \tilde{I}_{mm''}^l(\alpha, \mathbf{R}_I, \mathbf{R}_{I'}) . \quad (36)$$

to obtain a slightly more succinct form

$$S\left(\rho_{\text{mol}}, \hat{R}\rho'_{\text{mol}}\right) = \sum_{l, m, m''} I_{mm''}^l D_{mm''}^l(\hat{R}) \quad (37)$$

which we will not adapt here as it obfuscates the sums that nicely emphasize the series expansion over the indices l , m , and m' as well as the pairwise nuclear interaction over the indices I and I' .

We recall from Eq. (26) that the integral of the overlap defines the kernel. For $n = 2$, the rotationally invariant kernel is

$$\begin{aligned} k(\rho_{\text{mol}}, \rho'_{\text{mol}}; 2) &= \int \left| S\left(\rho_{\text{mol}}, \hat{R}\rho'_{\text{mol}}\right) \right|^2 d\Omega \\ &= \int d\Omega S\left(\rho_{\text{mol}}, \hat{R}\rho'_{\text{mol}}\right)^* S\left(\rho_{\text{mol}}, \hat{R}\rho'_{\text{mol}}\right) \\ &= \sum_{I, I'} \sum_{\substack{l, m, m' \\ \lambda, \mu, \mu'}} \tilde{I}_{mm'}^{l*} \tilde{I}_{\mu\mu'}^\lambda \underbrace{\int d\Omega D_{mm'}^l(\hat{R})^* D_{\mu\mu'}^\lambda(\hat{R})}_{\text{Wigner's orth. relation}} \\ &= \sum_{I, I'} \sum_{l, m, m'} \frac{1}{2l+1} \tilde{I}_{mm'}^{l*} \tilde{I}_{mm'}^l \end{aligned} \quad (38)$$

where we used new indices to avoid the doubly primed m'' and where by virtue of Wigner's orthogonality relation, we have

$$\begin{aligned} \int_0^{2\pi} d\alpha \int_0^\pi d\beta \sin\beta \int_0^{2\pi} d\gamma \frac{1}{8\pi^2} D_{m'k'}^{j'}(\hat{R}(\alpha, \beta, \gamma))^* D_{mk}^j(\hat{R}(\alpha, \beta, \gamma)) \\ = \frac{1}{2j+1} \delta_{m'm} \delta_{k'k} \delta_{j'j} \end{aligned} \quad (39)$$

We see that the Greek indices collapse with the Latin ones, $m \leftarrow \mu$, $m' \leftarrow \mu'$, and $l \leftarrow \lambda$.

The kernel is eventually defined with a power ζ , which is also a hyperparameter as it steers the sensitivity to the kernel changing the atomic positions and we set to unity to not obfuscate the results further. Finally, a normalization is introduced,

$$K(\rho_{\text{mol}}, \rho'_{\text{mol}}; n, \zeta) = \left(\frac{k(\rho_{\text{mol}}, \rho'_{\text{mol}}; n)}{\sqrt{k(\rho_{\text{mol}}, \rho_{\text{mol}}; n)k(\rho'_{\text{mol}}, \rho'_{\text{mol}}; n)}} \right)^\zeta \quad (40)$$

where each density is depending on the width α of the Gaussians and on the positions of the atoms, $\{\mathbf{R}_I\}$.

Due to the quadratic scaling of the integrals (for each pair of atoms in the scaffold), it can become inefficient for larger molecules. This is certainly true for very large molecules. A remedy for the quadratic scaling is proposed that involves an approximation in terms of an expansion using radial basis

functions. However, no systematic study has ever scrutinized this radial-basis approximation versus the analytic solution, apart from an initial discussion in the original paper.⁵ A further analysis of the accuracy of the power spectrum or engineered adversarial problems is beyond the scope of this analysis.

5.2 Electron Density Based Comparison: SOED

Instead of attaching a Gaussian function to each atomic position to introduce a fuzzy atomic core as a component of a molecular scaffold density as in Eq. (13), one is tempted to exploit the electron density of a molecule for the assessment of molecular similarity. Not only does this quantity relate to the electronic energy through the Hohenberg-Kohn theorem,³¹ it is also an observable that is accessible in diffraction experiments and from any quantum chemical method. Moreover, it also includes a representation of the atomic cores because its maxima indicate the nuclear positions (and even the nuclear charge by virtue of the Kato cusp condition). In addition to this information about the molecular scaffold, the electron density encodes information about the electronic wave function in the valence regions – although their peculiarities are in the tiny details and might require derived fields (such as the Laplacian⁴⁶) to be clearly visible.

In this context, it is important to emphasize that the electron density is typically calculated from absolute squares of molecular orbitals which are decomposed into atomic orbitals centered on the atomic nuclei. These atomic orbitals can then be represented by standard Gaussian functions available from a basis set library. In this regard, to employ the electron density is even on a technical level very similar to the SOAP scheme based on the molecular scaffold density — although the derivation will be far more difficult as we will see in the following. Hence, the electron density could be taken as a replacement for the molecular scaffold density to represent structural information as does SOAP (best seen with width parameters, α_I , that are different for every atomic core), but now also to encode electronic information.

Already the simplest electronic structure model will allow us to combine the atomic orbitals located at the nuclear positions linearly to yield molecular orbitals and to then yield the electron density, in complete analogy to Eq. (13). However, note that the molecular orbitals themselves cannot be used to replace the electron density or the molecular scaffold density because the coefficients in the LCAO expansion can take negative values and, in a superposition of molecular orbitals, these molecular orbital coefficients would cancel each other and all information about individual molecular orbitals will be lost. Obviously, this problem does not occur for the electron density that is taken as a weighted sum of the absolute squares of the molecular orbitals (see below).

If the additional electronic structure information encoded in the electron density can be harnessed, it might be better suited as a descriptor than SOAP, which only encodes the molecular scaffold. A similar reasoning has led Carbó⁴⁷ in the context of cheminformatics to develop a similarity measure based on the

overlap of electron density, which is sometimes called the Carbo index r_{AB} ,

$$r_{AB} = \frac{\int_V \rho_A \rho_B d\mathbf{r}}{(\int_V \rho_A^2 d\mathbf{r})^{1/2} (\int_V \rho_B^2 d\mathbf{r})^{1/2}} \quad (41)$$

and therefore reminiscent of Eq. (40) in the SOAP formalism. The derivation, where the first steps are similar to ours, is presented in the Appendix of Ref. 47 but leaves out the key step of density rotations introduced in SOAP. The optimum overlap of r_{AB} is numerically calculated whereas we aim at an analytical solution. However, bringing electron densities in a rotatable form in a single-center picture leads to significant mathematical overhead as we shall see in the following.

Since we assume that we will always have results for a simple electronic structure model available from which we may take test data, we consider a single Slater determinant model. For such an ansatz, which is the basis of Kohn-Sham DFT, Hartree-Fock theory, and any approximate Hartree-Fock model, the electron density is the square of w molecular orbitals, $\phi_i(\mathbf{r})$, where \mathbf{r} is the coordinate of the electron,

$$\rho_{\text{el}}(\mathbf{r}) = \sum_{i=1}^w n_i |\phi_i(\mathbf{r})|^2 \quad (42)$$

with occupation numbers n_i (that may be taken to be one in an unrestricted framework, where w will then be identical to the number of electrons N). The MOs are usually expanded as a linear combination of atomic orbitals (LCAO),

$$\phi_i(\mathbf{r}) = \sum_A^M \sum_{\mu \in A} c_{\mu}^{(i)} \chi_{\mu}(\mathbf{r}) , \quad (43)$$

as in Eq. (3), but now with an explicit notion of the atom (' A ') on which a function χ_{μ} is centered. In other words, the above expression introduces explicitly a sum over these atomic centers of the basis functions, which we may denote with the German word 'Aufpunkt' in order to introduce a notion that allows for centers that are not identical with nuclear positions. Hence, there is still a total of m basis functions (i.e., the atomic orbitals (AOs) in this linear combination of atomic orbitals), $\chi_{\mu}(\mathbf{r})$, and their corresponding coefficients are $c_{\mu}^{(i)}$. Gaussian orbitals (GTOs) employed as AO are defined as

$$\chi_{\mu}(\mathbf{r}_A) = N_{\mu} f_{\mu}(\mathbf{r}_A) g_{\mu}(\mathbf{r}_A) \quad (44)$$

with the polynomial

$$f_{\mu}(\mathbf{r}_A) = |\mathbf{r}_A|^{L_{\mu}} Y_{L_{\mu} M_{\mu}}(\Omega_{\mathbf{r}_A}) , \quad (45)$$

the Gaussian

$$g_{\mu}(\mathbf{r}_A) = \exp\left(-\zeta_{\mu} |\mathbf{r}_A|^2\right) , \quad (46)$$

and with the normalization constant N_μ . Furthermore, we have the local vector from nucleus A at \mathbf{R}_A to the field variable \mathbf{r} (see Figure 7), i.e., $\mathbf{r}_A = |\mathbf{r} - \mathbf{R}_A|$, the spherical harmonic, $Y_{L_\mu M_\mu}(\Omega_{\mathbf{r}_A})$, which is also centered at the position of nucleus A and hence in the local coordinate system \mathbf{e}'_{x_A} , \mathbf{e}'_{y_A} , and \mathbf{e}'_{z_A} , with orbital quantum number (degree) L_μ and magnetic quantum number (order) M_μ , and polar angles $\Omega_{\mathbf{r}_A} = (\theta_{\mathbf{r}_A}, \phi_{\mathbf{r}_A})$ with respect to nucleus at \mathbf{R}_A , and effective nuclear charge ζ_μ . In the following, we omit the variable dependence for the sake of brevity, i.e., $\chi_\mu \equiv \chi_\mu(\mathbf{r})$. As before, we will have to bring this multi-centered approach into a framework where all angles are to be taken with respect to a single center, which facilitates the rotation operation and which is taken to be the center of mass.

Substituting the AO expansion, Eq. (43), into the density expression, Eq. (42), we obtain

$$\rho_{\text{el}}(\mathbf{r}) = \sum_i^w \sum_{A,B}^M \sum_{\substack{\mu \otimes A \\ \nu \otimes B}} n_i c_\mu^{(i)} c_\nu^{(i)} \chi_\mu \chi_\nu \quad (47)$$

with basis functions (i.e., 'AOs') χ_μ and χ_ν and expansion coefficients $c_\mu^{(i)}$ and $c_\nu^{(i)}$. As usual, the introduction of a density matrix,

$$D_{\mu\nu} = \sum_i^w n_i c_\mu^{(i)} c_\nu^{(i)} \quad (48)$$

(which is not to be confused with the Wigner D-matrices) brings the expression for the electron density into a more compact form,

$$\rho_{\text{el}}(\mathbf{r}) = \sum_{A,B}^M \sum_{\substack{\mu \otimes A \\ \nu \otimes B}} D_{\mu\nu} \chi_\mu \chi_\nu . \quad (49)$$

Moreover, for notational convenience we introduce a product GTO,

$$\chi_{\mu\nu}(\mathbf{r}_A, \mathbf{r}_B) = N_{\mu\nu} f_\mu(\mathbf{r}_A) f_\nu(\mathbf{r}_B) g_\mu(\mathbf{r}_A) g_\nu(\mathbf{r}_B) \quad (50)$$

with the normalization constant $N_{\mu\nu} = N_\mu N_\nu$

Since we want to rotate one of the electron densities with respect to the other, the expression must be made dependent on the rotation angles. However, as in the case of SOAP, the angles in the spherical harmonics are defined with respect to the local coordinate system at a nucleus, but must be defined with respect to a single center that will be the center of mass. For this, we follow the derivation of Kaufmann and Baumeister⁴⁴ here. However, the result from the exact derivation, which we sketch in the supporting information, is very long-winded and turns out to be computationally costly to evaluate. Therefore, we propose two ways of approximating the GTO in order to simplify the expression: First, we neglect all products of higher order spherical harmonics; e.g., no

product of two p functions was considered, if they are positioned at different nuclei. Whereas this simplifies the derivation, it is still very involved. Therefore, we eliminate the polynomial factors by replacing all p basis functions with lobe functions, i.e., s -type functions with shifted centers that resemble functions of higher angular momentum quantum number (see supporting information for details on how these new Aufpunkte were determined by starting from the nuclear positions). This is also possible for higher-orbital-momentum functions such as d functions. In this way, we generate an all- s -type basis set that sufficiently well represents the electron density and for which the calculated MO coefficients can be inherited. Note that, from a technical point of view, the new Aufpunkte of these lobe functions are then to be treated as (new artificial) nuclear positions in the evaluation procedure for SOAP and, therefore, SOED can now be evaluated with a SOAP-type procedure.

By virtue of the Gaussian product theorem, each product of the two Gaussians χ_μ and χ_ν in Eq. (49) becomes another Gaussian. Hence, we can collapse the double indices $\mu\nu$ in Eq. (49) into a single index, which we call \tilde{I} in order to associate it to the corresponding expression in the SOAP derivation: since we consider a lobe-basis of s -functions only, we obtain the electron density as an expansion into s -functions only with Aufpunkte given at positions denoted by \tilde{I} , some of which are actual nuclear positions:

$$\rho_{\text{el}}(\mathbf{r}) = \sum_{\tilde{I}}^{\tilde{m}} D_{\tilde{I}} \chi_{\tilde{I}} \quad (51)$$

All of these positions \tilde{I} are subject to the SOAP rotation and overlap procedures and can be treated like ghost atoms. Hence, we have recovered a generalized version of SOAP with weights $D_{\tilde{I}}$ in front of the basis functions \tilde{I} , each of which will, in general, carry a different exponent (rather than a common exponent α that is the standard choice for SOAP). Recall that the weights $D_{\tilde{I}}$ contain products of MO coefficients and occupation numbers (or first-order reduced density matrices), which can be determined in an electronic structure calculation (e.g., in a Hartree-Fock calculation). Of course, this will require one storing electronic structure data in addition to the nuclear coordinates of a molecule, but that should no present a hurdle as the molecular structures will typically be optimized with an electronic structure method whose wave-function ingredients then simply need to accompany the Cartesian coordinates in a data base in order to be exploited by a machine learning ansatz based on SOED.

Finally, we obtain, by virtue of the direct analogy with SOAP, for the overlap of two electron densities,

$$k(\rho_{\text{el}}, \rho'_{\text{el}}; 2) = \sum_{\tilde{I}, \tilde{I}'}^{\tilde{m}, \tilde{m}'} \sum_{l, m, m'} \frac{D_{\tilde{I}}^2 D_{\tilde{I}'}^2}{2l+1} \tilde{I}_{mm'}^{l*} \tilde{I}'_{mm'}^l \quad (52)$$

5.3 Numerical Comparison of SOAP and SOED

We show in Figure 8 a comparison for the SOAP and SOED similarity results for the reactions in Figure 1. On both axes are the reactant (R), the TS (T), and the product (P) of the reaction. The diagonal is 1, as self-similarity is perfect by design. The first row shows SOAP and the second row shows the SOED results. As one can see, the electron density based descriptor is more sensitive to the reaction progress, because it drops from reactant to TS more than traditional SOAP. Again, the reactant and the TS are more similar in all descriptors shown than TS and product, implying an early TS again, as we already found for the Coulomb matrix and the energy diagram. However, product and TS are less similar than product and reactant, which seems unexpected at first sight. However, we note that this is actually reasonable if a purely structure based descriptor that is largely independent of directional information (owing to the radial Gaussians involved in SOAP) favors similarity in terms of equilibrium bond lengths over similarity between stretched and equilibrium bond lengths in one constitutional isomer.

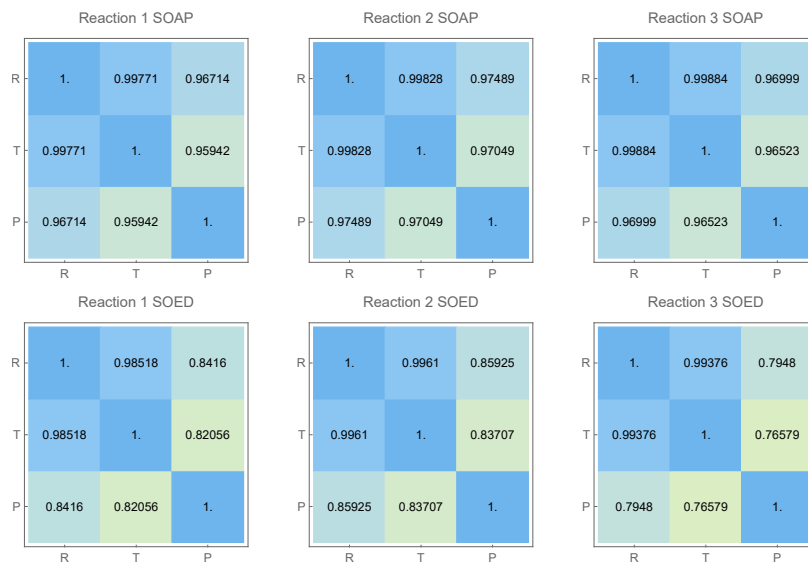


Figure 8: Comparison of SOAP (top panel) and SOED (bottom panel) for the three test reactions; 'R' denotes the reactant, 'T' the transitions state, and 'P' the product.

One reason for the larger dissimilarity obtained for the SOED kernel is the fact that the parameter in the exponent of the Gaussian functions is no longer a hyperparameter. By contrast to SOAP with a fixed value α for all nuclei, the analogous parameter in a Gaussian basis set that describes the atomic orbitals is fixed to represent these orbitals. In order to demonstrate how sensitive SOAP

is in this respect, a comparison of SOAP results are shown in Figure 9 that were obtained for the three reactions with varying α : $\alpha = 1$, $\alpha = 10$, and $\alpha = 100$ (recall that the standard value is $\alpha = 0.4$). It is apparent from Figure 9, when rotating one SOAP scaffold density with respect to the other, narrower peaks will have less overlap compared to when they are spread out.

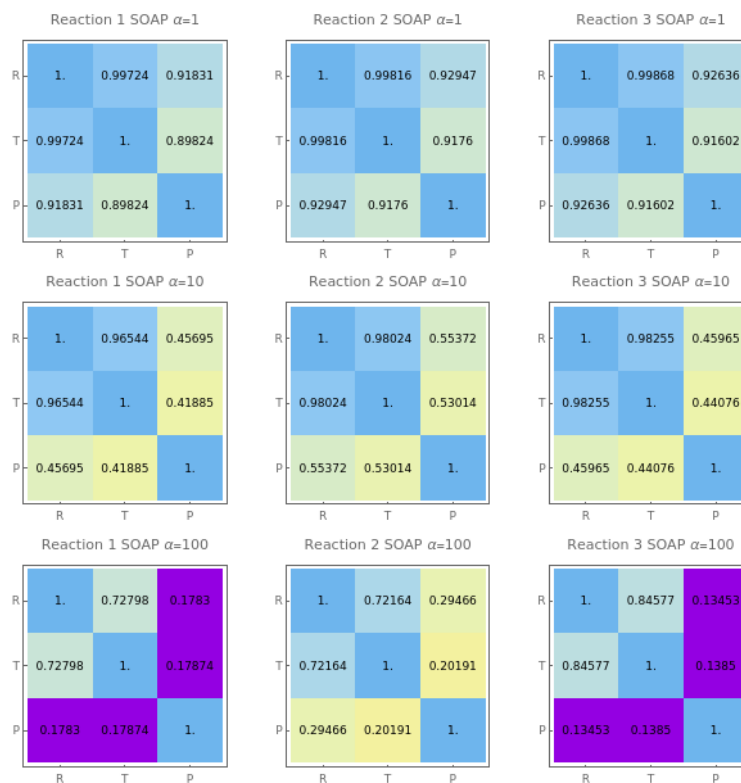


Figure 9: Comparison of SOAP for three different values of the common exponent α for the three test reactions; 'R' denotes the reactant, 'T' the transitions state, and 'P' the product.

6 Conclusions

In this work, we considered an elementary expression for the electronic energy that allowed us to discuss two widely used descriptors of molecular similarity in machine learning from the point of view of electronic structure theory: Coulomb matrix and SOAP. We showed how to ground their definitions into electronic structure theory by (i) introducing Coulomb lists that allowed us to scrutinize the rather arbitrary diagonal entries of the Coulomb matrix and its intransparent diagonalization step and by (ii) relating the fuzzy density that encodes molecular structure for SOAP to the actual electron density, which then also carries electronic structure information directly into the descriptor.

Our formal discussion was accompanied by a single example that served the purpose to illustrate the results one obtains with the standard descriptors Coulomb matrix and SOAP and with our new descriptors Coulomb list and SOED. The single example was chosen to provide structures connected through an elementary reaction step: reactant, transition state, product; i.e., structures that are rather similar by definition and that occur in chemical reaction networks. This example allowed us to study the variation of the descriptors along a coordinate that connects the three types of structures. Whereas structural change is therefore continuous, the electronic structure is different, which is the reason why the transition state structure acquires a higher energy than the reactant and product structures. This situation therefore introduces a peculiar twist that would allow one to argue that the transition state structure is more similar to either product and reactant than product and reactant are similar to one another, while the difference in electronic structure prompts one to argue that the stable intermediates, i.e., product and reactant, should be more similar to one another with respect to the nature of their electronic structures.

For the Coulomb list, we found that the $\mathcal{F}_n^{(J)}$ descriptor yields interpretable traces by contrast to the convoluted eigenvalues of the Coulomb matrix. At the same time, it contained the same information and can therefore replace the Coulomb-matrix eigenvalue features, alleviating also the need for the diagonalization step.

We emphasize that traces of these features along reaction coordinates clearly correlated with the change in molecular structure and are able to identify the transition state structure in the feature. Hence, the electronic difference of the transition state compared to the stable intermediates (reactant and product) will be detectable in these features, if they are considered relative to one another. However, this was not possible for SOAP and SOED.

We found that SOED is more sensitive than SOAP with the standard α parameter. This is a consequence of the widths of the Gaussians that are present in the representation of the electron density. We found that narrowing the Gaussians that compose the SOAP kernel also increases sensitivity, so that SOAP, which is much easier to evaluate than SOED, could be used instead, but with a parameter α in the exponent that is larger than the standard one.

In future work, we will build upon these findings and elaborate on molecular similarity in the context of a huge number of molecular structures occurring in

a large reaction network.

Acknowledgements

Financial support by the Swiss National Science Foundation through project no. 200021_182400 is gratefully acknowledged.

Appendix: Computational Methodology

The quantum chemical calculations for the model reactions were carried out with Orca 5.⁴⁸ We performed unrestricted Kohn–Sham PBE⁴⁹ structure optimizations with the SVP basis set with density fitting.⁵⁰ Our molecular similarity descriptors were then obtained from Hartree-Fock single-point calculations. The atomic descriptors $\mathcal{F}_n^{(J)}$ and $\mathcal{F}_e^{(J)}$ were obtained with the program Serenity,^{51,52} which calculated the nuclear attraction integrals contracted with the density matrix elements and the nucleus–electron interaction with unrestricted Kohn–Sham PBE⁴⁹ and the def2-SVP basis set.⁵³

For SOED, we obtained the molecular orbital coefficients for the electron density in Hartree–Fock calculations with the tiny STO-3G basis set⁵⁴ with Gaussian,⁵⁵ where the keyword `Integral(SplitSP)` had to be applied to not obtain `S=P` contracted orbitals but regular s and p orbitals. We note that despite its small size, this basis set already produces the main features of the electron density (non-isotropic local effects through minimal polarization by basis functions on atomic neighbors and an element-specific maximum of the density distribution at the various atomic nuclei) that makes SOED different from SOAP.

We implemented Eq. (26), the SOAP kernel, in Mathematica⁵⁶ and this code is available from the authors. In addition, we established a python implementation for routine applications that will be made available open source. In our implementation, we used NumPy⁵⁷ array programming (vectorization). The data structure `ndarray` harnesses the CPU’s SIMD (Single Instruction, Multiple Data) architecture for a significant speed-up compared to a loop-based implementation. Furthermore, we parallelized the calculation with the library Ray.⁵⁸

According to Eq. (34), the overlap for the SOAP procedure is dependent on an infinite sum that originates from the Rayleigh expansion in Eq. (15) and the rotation of the spherical harmonics as an expansion of Wigner-D matrices in Eq. (23), which converges uniformly. Even though we avoid the standard power spectrum approximation, which would introduce another approximation, we can only approach the exact overlap within numerical accuracy. As the authors of the original paper⁵ noted, the pairwise evaluation for all I and I' leads to a big computational overhead. Since we approximated the p -functions by (lobe) s -functions, very many terms are created in this double sum. Our largest molecule from reaction 3 in Figure 1 then requires 333 s -functions. For this reason, it is

hard to reach a high l in the expansion, as m and m' range from $-l$ to l in steps of one. Hence, for the results presented in Figure 8, the maximum value for l was 3 for SOED and 5 for SOAP.

In the original reference introducing SOAP,⁵ it had already been noted that the computation of SOAP can be expensive, since the terms inside the sums of Eq. 38 have to be evaluated for each pairwise interaction of atoms. The sums over l , m , and m' scale with $O(L_{\max}^3)$, where L_{\max} is the truncation of the infinite sum over l , yielding an overall complexity of $O(M^2 L_{\max}^3)$. In SOED, Eq. (52), where the density is based on m^2 basis functions for each density, the evaluation becomes even more expensive as $O(m^4 L_{\max}^3)$, where the number of basis functions, m , is in all practical cases much bigger than the number of atoms, M . The straightforward way to treat this unfavorable scaling is to trade off accuracy for speed and reduce L_{\max} . For all but the smallest molecules, larger basis sets than those on the order of STO-3G will likely not be feasible. As in SOAP with the power spectrum, it might be possible to simplify the nested sum with some mathematical transformations to gain a speed-up.

References

- [1] C. M. BISHOP, *Pattern Recognition and Machine Learning*, Information Science and Statistics, Springer, 2006.
- [2] J. MERCER and A. R. FORSYTH, *Philosophical Transactions of the Royal Society of London. Series A, Containing Papers of a Mathematical or Physical Character* **209**, 415 (1909).
- [3] T. HASTIE, R. TIBSHIRANI, and J. FRIEDMAN, *The Elements of Statistical Learning*, Springer Series in Statistics, Springer New York Inc., 2001.
- [4] C. E. RASMUSSEN and C. K. I. WILLIAMS, *Gaussian Processes for Machine Learning*, Adaptive Computation and Machine Learning, MIT Press, 2006.
- [5] A. P. BARTÓK, R. KONDOR, and G. CSÁNYI, *Phys. Rev. B* **87**, 184115 (2013).
- [6] R. TODESCHINI and V. CONSONNI, *Molecular Descriptors for Chemoinformatics*, Methods and Principles in Medicinal Chemistry, Wiley, 2009.
- [7] K. HANSEN, F. BIEGLER, R. RAMAKRISHNAN, W. PRONOBIS, O. A. VON LILIENFELD, K.-R. MÜLLER, and A. TKATCHENKO, *J. Phys. Chem. Lett.* **6**, 2326 (2015).
- [8] B. HUANG and O. A. VON LILIENFELD, *Nat. Chem.* **12**, 945 (2020).
- [9] A. S. CHRISTENSEN, L. A. BRATHOLM, F. A. FABER, and O. ANATOLE VON LILIENFELD, *J. Chem. Phys.* **152**, 044107 (2020).

- [10] M. RUPP, A. TKATCHENKO, K.-R. MÜLLER, and O. A. VON LILIENFELD, *Phys. Rev. Lett.* **108** (2012).
- [11] K. HANSEN, G. MONTAVON, F. BIEGLER, S. FAZLI, M. RUPP, M. SCHEFFLER, O. A. VON LILIENFELD, A. TKATCHENKO, and K.-R. MÜLLER, *J. Chem. Theory Comput.* **9**, 3404 (2013).
- [12] J. SCHRIER, *J. Chem. Inf. Model.* **60**, 3804 (2020).
- [13] B. HUANG and O. A. VON LILIENFELD, *J. Chem. Phys.* **145**, 161102 (2016).
- [14] C. R. COLLINS, G. J. GORDON, O. A. VON LILIENFELD, and D. J. YARON, *J. Chem. Phys.* **148**, 241718 (2018).
- [15] S. DE, A. P. BARTÓK, G. CSÁNYI, and M. CERIOTTI, *Phys. Chem. Chem. Phys.* **18**, 13754 (2016).
- [16] M. J. WILLATT, F. MUSIL, and M. CERIOTTI, *J. Chem. Phys.* **150**, 154110 (2019).
- [17] F. MUSIL, A. GRISAFI, A. P. BARTÓK, C. ORTNER, G. CSÁNYI, and M. CERIOTTI, *Chem. Rev.* **121**, 9759 (2021).
- [18] A. P. BARTÓK, S. DE, C. POELKING, N. BERNSTEIN, J. R. KERMODE, G. CSÁNYI, and M. CERIOTTI, *Sci. Adv.* **3**, e1701816 (2017).
- [19] M. CERIOTTI, C. CLEMENTI, and O. ANATOLE VON LILIENFELD, *J. Chem. Phys.* **154**, 160401 (2021).
- [20] S. N. POZDNYAKOV, M. J. WILLATT, A. P. BARTÓK, C. ORTNER, G. CSÁNYI, and M. CERIOTTI, *Phys. Rev. Lett.* **125**, 166001 (2020).
- [21] F. MUSIL and M. CERIOTTI, *CHIMIA* **73**, 972 (2019).
- [22] A. GOSCINSKI, G. FRAUX, G. IMBALZANO, and M. CERIOTTI, *Mach. Learn.: Sci. Technol.* **2**, 025028 (2021).
- [23] A. GRISAFI, A. FABRIZIO, B. MEYER, D. M. WILKINS, C. CORMINBOEUF, and M. CERIOTTI, *ACS Cent. Sci.* **5**, 57 (2019).
- [24] A. FABRIZIO, K. BRILING, A. GRISAFI, and C. CORMINBOEUF, *Chimia* **74**, 232 (2020).
- [25] K. ABDELFAH, W. YANG, R. V. SOLOMON, B. RAJBANSHI, A. CHOWDHURY, M. ZARE, S. K. KUNDU, A. YONGE, A. HEYDEN, and G. TEREJANU, *J. Phys. Chem. C* **123**, 29804 (2019).
- [26] D. LEMM, G. F. VON RUDORFF, and O. A. VON LILIENFELD, *Nat. Commun.* **12**, 4468 (2021).
- [27] R. JACKSON, W. ZHANG, and J. PEARSON, *Chem. Sci.* **12**, 10022 (2021).

- [28] J. ZHANG, Y.-K. LEI, Z. ZHANG, X. HAN, M. LI, L. YANG, Y. I. YANG, and Y. Q. GAO, *Phys. Chem. Chem. Phys.* **23**, 6888 (2021).
- [29] R. RAMAKRISHNAN, P. O. DRAL, M. RUPP, and O. A. VON LILIENFELD, *Sci. Data* **1**, 140022 (2014).
- [30] N. C. HANDY, Density Functional Theory, in *Lecture Notes in Quantum Chemistry II: European Summer School in Quantum Chemistry*, edited by B. O. ROOS, Lecture Notes in Chemistry, pp. 91–124, Springer, 1994.
- [31] P. HOHENBERG and W. KOHN, *Phys. Rev.* **136**, B864 (1964).
- [32] R. RAMAKRISHNAN, M. HARTMANN, E. TAPAVICZA, and O. A. VON LILIENFELD, *J. Chem. Phys.* **143**, 084111 (2015).
- [33] R. G. PARR and Y. WEITAO, *Density-Functional Theory of Atoms and Molecules*, International Series of Monographs on Chemistry, Oxford University Press, 1995.
- [34] O. A. VON LILIENFELD, *Int. J. Quantum Chem.* **113**, 1676 (2013).
- [35] J. E. MEANY, V. MINDERHOUT, and Y. PÖCKER, *J. Chem. Educ.* **78**, 204 (2001).
- [36] J. E. MOUSSA, *Phys. Rev. Lett.* **109**, 059801 (2012).
- [37] W. J. SZLACHTA, A. P. BARTÓK, and G. CSÁNYI, *Phys. Rev. B* **90**, 104108 (2014).
- [38] N. RAIMBAULT, A. GRISAFI, M. CERIOTTI, and M. ROSSI, *New J. Phys.* **21**, 105001 (2019).
- [39] V. L. DERINGER, C. J. PICKARD, and G. CSÁNYI, *Phys. Rev. Lett.* **120**, 156001 (2018).
- [40] G. FERRÉ, T. HAUT, and K. BARROS, *J. Chem. Phys.* **146**, 114107 (2017).
- [41] E. A. ENGEL, A. ANELLI, A. HOFSTETTER, F. PARUZZO, L. EMSLEY, and M. CERIOTTI, *Phys. Chem. Chem. Phys.* **21**, 23385 (2019).
- [42] G. N. WATSON, *A Treatise on the Theory of Bessel Functions*, Cambridge University Press, 1995.
- [43] H. WEBER, **1868**, 222 (1868).
- [44] K. KAUFMANN and W. BAUMEISTER, *J. Phys. B: At. Mol. Opt. Phys.* **22**, 1 (1989).
- [45] A. P. BARTÓK, R. KONDOR, and G. CSÁNYI, *Phys. Rev. B* **96**, 019902 (2017).
- [46] P. L. A. POPELIER, *Coord. Chem. Rev.* **197**, 169 (2000).

- [47] R. CARBÓ, L. LEYDA, and M. ARNAU, *Int. J. Quantum Chem.* **17**, 1185 (1980).
- [48] F. NEESE, F. WENNMOHS, U. BECKER, and C. RIPLINGER, *J. Chem. Phys.* **152**, 224108 (2020).
- [49] J. P. PERDEW, K. BURKE, and M. ERNZERHOF, *Phys. Rev. Lett.* **77**, 3865 (1996).
- [50] F. WEIGEND, *Phys. Chem. Chem. Phys.* **8**, 1057 (2006).
- [51] J. P. UNSLEBER, T. DRESSELHAUS, K. KLAHR, D. SCHNIEDERS, M. BÖCKERS, D. BARTON, and J. NEUGEBAUER, *J. Comput. Chem.* **39**, 788 (2018).
- [52] D. BARTON, M. BENSBERG, M. BÖCKERS, T. DRESSELHAUS, P. ESCHENBACH, L. HELLMANN, K. KLAHR, A. MASSOLLE, N. NIEMEYER, D. SCHNIEDERS, J. TÖLLE, J. P. UNSLEBER, and J. NEUGEBAUER, Qcserenity/Serenity: Release 1.3.1, 2020.
- [53] F. WEIGEND and R. AHLRICHS, *Phys. Chem. Chem. Phys.* **7**, 3297 (2005).
- [54] W. J. HEHRE, R. F. STEWART, and J. A. POPLE, *J. Chem. Phys.* **51**, 2657 (1969).
- [55] M. J. FRISCH, G. W. TRUCKS, H. B. SCHLEGEL, G. E. SCUSERIA, M. A. ROBB, J. R. CHEESEMAN, G. SCALMANI, V. BARONE, G. A. PETERSON, H. NAKATSUJI, X. LI, M. CARICATO, A. V. MARENICH, J. BLOINO, B. G. JANESKO, R. GOMPERTS, B. MENNUCCI, H. P. HRATCHIAN, J. V. ORTIZ, A. F. IZMAYLOV, J. L. SONNENBERG, D. WILLIAMS-YOUNG, F. DING, F. LIPPARINI, F. EGIDI, J. GOINGS, B. PENG, A. PETRONE, T. HENDERSON, D. RANASINGHE, V. G. ZAKRZEWSKI, J. GAO, N. REGA, G. ZHENG, W. LIANG, M. HADA, M. EHARA, K. TOYOTA, R. FUKUDA, J. HASEGAWA, M. ISHIDA, T. NAKAJIMA, Y. HONDA, O. KITAO, H. NAKAI, T. VREVEN, K. THROSSELL, J. A. MONTGOMERY, JR., J. E. PERALTA, F. OGLIARO, M. J. BEARPARK, J. J. HEYD, E. N. BROTHERS, K. N. KUDIN, V. N. STAROVEROV, T. A. KEITH, R. KOBAYASHI, J. NORMAND, K. RAGHAVACHARI, A. P. RENDELL, J. C. BURANT, S. S. IYENGAR, J. TOMASI, M. COSSI, J. M. MILLAM, M. KLENE, C. ADAMO, R. CAMMI, J. W. OCHTERSKI, R. L. MARTIN, K. MOROKUMA, O. FARKAS, J. B. FORESMAN, and D. J. FOX, Gaussian~16 Revision C.01, 2016.
- [56] W. R. INC., Mathematica, Version 13.0.0, Champaign, IL, 2021.
- [57] C. R. HARRIS, K. J. MILLMAN, S. J. VAN DER WALT, R. GOMMERS, P. VIRTANEN, D. COURNAPEAU, E. WIESER, J. TAYLOR, S. BERG, N. J. SMITH, R. KERN, M. PICUS, S. HOYER, M. H. VAN KERKWIJK, M. BRETT, A. HALDANE, J. F. DEL RÍO, M. WIEBE, P. PETERSON,

- P. GÉRARD-MARCHANT, K. SHEPPARD, T. REDDY, W. WECKESSER, H. ABBASI, C. GOHLKE, and T. E. OLIPHANT, *Nature* **585**, 357 (2020).
- [58] P. MORITZ, R. NISHIHARA, S. WANG, A. TUMANOV, R. LIAW, E. LIANG, M. ELIBOL, Z. YANG, W. PAUL, M. I. JORDAN, and I. STOICA, Ray: A Distributed Framework for Emerging AI Applications, 2018.